The Triply-Folded Horn Reflector: A Compact Ground Station Antenna Design for Satellite Communications

By A. J. GIGER and R. H. TURRIN

(Manuscript received May 20, 1965)

An antenna suitable for ground stations of satellite communications systems is described. The antenna has very good low-noise properties, high aperture efficiency, and excellent broadband characteristics. It can be operated without a radome and allows the location of all communications and tracking equipment in a stationary room on the ground. Called the "triply-folded horn-reflector antenna," it is derived from the well-known conical horn-reflector antenna by folding the horn three times to bring its apex into a stationary position on the ground. Plane reflectors are used in the folding process and the propagation in the antenna is based on the principles of geometrical optics.

The paper describes electrical tests on an antenna model at frequencies of 60 and 11 gc and presents results of hydrodynamic tests which were performed to study the behavior of the antenna in high wind.

I. INTRODUCTION

Among the antennas suitable for ground stations of a satellite communications system, the horn reflector is highly desirable since it unites in one design such electrical characteristics as high-aperture efficiency, low-noise temperature, immunity from interfering signals and extreme broadband capabilities. High-aperture efficiency results from guiding the fundamental mode electromagnetic energy from the focal point by means of the horn directly to the parabolic reflector. In this way the aperture field distribution is not strongly tapered and energy loss due to spillover is minimized. The low noise temperature and immunity from interference results mainly from the inherent shielding afforded by the horn-reflector structure.

Both the pyramidal and conical horn-reflector antenna designs have

been investigated and applied in the past few years.[1,2,3] Notable among the applications is the large conical horn-reflector antenna at the ground station for satellite communications near Andover, Maine. The conical horn structure was chosen for this application because of its structural and electrical advantages. While this antenna has performed well, a number of areas exist where improvements would be desirable. For instance, the need for carrying large amounts of equipment on the rotating structure of the antenna contributes to its high weight and cost. Furthermore, the radome which is necessary for operation of a large horn-reflector antenna under high wind conditions, degrades antenna performance. During periods of rain or snow the radome seriously increases the thermal noise and the signal loss in the communications system.

It is the purpose of this paper to describe a new antenna structure which eliminates the major disadvantages of high weight and need for a radome, without seriously degrading its electrical or operational characteristics. Results of scale model studies of electrical and wind loading characteristics are presented and other aspects of this new design are discussed.

II. THE TRIPLY-FOLDED HORN-REFLECTOR ANTENNA

2.1 *The Configuration*

The new antenna configuration evolved from the conical horn-reflector antenna shown in Fig. 1(a). It is apparent that by using the principles of geometrical optics, the length of the structure can be reduced considerably by introducing a plane reflector R_1 in the horn as shown in Fig. 1(b). In this way, the apex of the horn which coincides with the "folded" focal point F_2 of the paraboloid can be located near the lower plane of the structure. A large rotating joint as shown in Fig. 1(b) is now necessary to permit elevation rotation of the paraboloidal reflector section. This configuration gives the advantage of consolidating the terminal equipment at one level instead of the two levels shown in Fig. 1(a). However, all the equipment still would be required to rotate with the structure in azimuth with the associated penalty of inertia and weight loading, as well as the complexities of feeding power and signal leads through slip rings or cable wraps.

A further extension of this concept consists of introducing two additional plane reflectors R_2 and R_3 to permit the axis of the horn apex section to coincide with the azimuth axis of rotation (Fig. 1(c)). Thus, by introducing another rotating joint near the apex, the final feed section

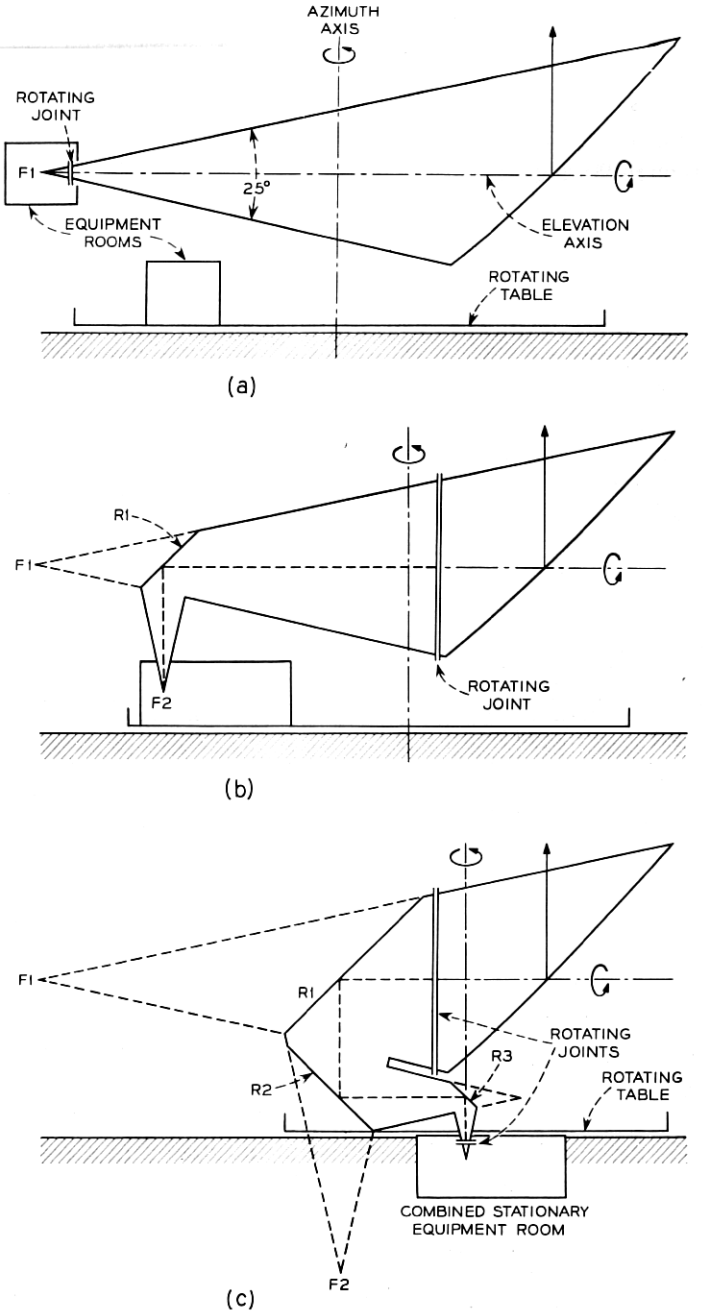

Fig. 1 — Development of the triply-folded horn geometry from the straight horn: (a) straight horn-reflector antenna; (b) single-fold intermediate stage; (c) triply-folded horn-reflector antenna design with horn apex coincident with the azimuth rotational axis.

can be made stationary and all of the terminal equipment mounted off the rotating antenna structure.

Although 90 degree reflections are shown in the triply-folded horn-reflector antenna of Fig. 1(c), the underlying principle of geometrical optics allows the use of reflection-angles other than 90 degrees.

2.2 *Operation Without Radome*

In order to eliminate the above mentioned transmission degradation during rain or snow, the triply-folded horn should be operated without a radome. The inherent compactness of the triply-folded horn antenna is a definite asset for achieving adequate satellite tracking during periods of high wind. A helpful by-product of the elimination of the detrimental radome effects is a reduction of the size of an uncovered antenna for given transmission requirements in the satellite system.

Several variations of the folded horn configuration were considered. As a result of hydrodynamic scale model tests, best resistance to high wind velocities was obtained by the configuration shown in Fig. 2. Here the azimuth axis is located to minimize the swept radius of the structure which includes an exterior fairing tightly fitted to the silhouette of the folded horn.

In environments such as Andover, Maine, means for melting snow and ice from the exposed parabolic reflector surface must be provided. One possible approach to this problem is the use of electrical deicing devices which can be zone controlled to localize heating effects. Another possibility consists of closing the aperture with a low-loss cover. While a wet aperture cover does not cause as great a transmission degradation as a radome, it should not be installed without some provisions for removing the water from its surface. Fig. 3 indicates a possible technique in which high-speed air is directed by nozzles tangentially over the cover to reduce or even blow away any possible water layer. A plenum is provided in the back of the cover where a slight over-pressure is produced by the blowers. Formed ducts, made of low-loss foam material which are designed according to aerodynamical principles and end in nozzles, accelerate the air to the high velocity required at the outside surface of the aperture cover.

2.3 *Mechanical Considerations*

The triply-folded conical horn-reflector antenna structure shown in Fig. 2 would be constructed of steel tubular members for the reflector panel supports and of standard rolled shapes of structural steel elsewhere.

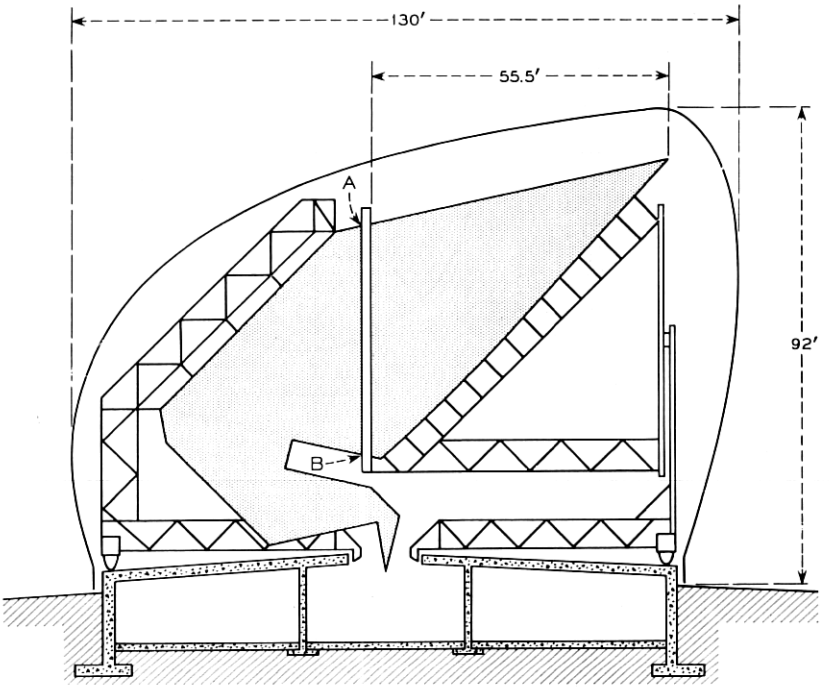

Fig. 2 — Cross sectional view of proposed triply-folded horn-reflector antenna showing asymmetrical outer fairing. The dimensions are for a 2250 square foot aperture size.

Aluminum would have disadvantages from a cost and fabrication viewpoint. When operating without an aperture cover, it is necessary for the parabolic reflector panels to be resistant to distortion under varying solar heating as the surface is exposed to rapidly varying sun and shadow. It also is necessary to melt ice and snow from the reflector. A stretch formed, single-skin aluminum panel would be suitable for this application rather than the aluminum honeycomb panels which were used at Andover. The honeycomb construction is vulnerable to serious warping if the outer skins are not at reasonably uniform temperatures and the core acts as an effective insulator against efficient heat transfer for snow and ice melting purposes. The single-skin aluminum panel would have to be about 50 per cent heavier than the equivalent honeycomb panel. The exterior fairing could be built of lightweight panels of aluminum or resin impregnated Fiberglas.

The entire structure rotates on a single circular track mounted on a

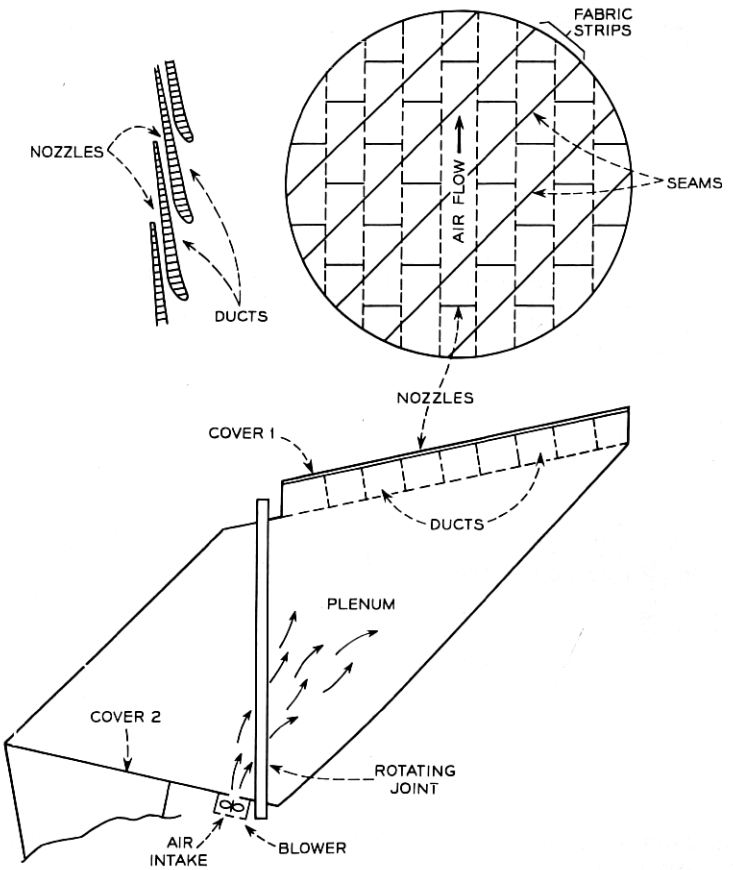

Fig. 3 — A method proposed to deflect precipitation from the aperture by means of high velocity air streams. Covers 1 and 2 might be Hypalon covered Dacron fabric similar to the Andover radome material but only 0.040 inch thick.

circular foundation. The foundation can incorporate enough living space to house all terminal equipment in an underground equipment area.

The overall RMS deflection of the four reflecting surfaces of the triply-folded horn should not exceed a value which depends on the maximum allowable gain degradation at the highest frequency of operation. The total allowable RMS deflection can be determined from formulas contained in Ref. 4. It is logical to divide the total RMS value among the reflecting surfaces such that the accuracy requirements increase from the largest to the smallest surface. A possible way of assigning the total RMS error, σ_{tot} among the four reflecting surfaces could be as follows: $\sigma_1 = 0.84\sigma_{tot}$, $\sigma_2 = 0.42\sigma_{tot}$, $\sigma_3 = 0.28\sigma_{tot}$, and $\sigma_4 = 0.21\sigma_{tot}$.

Aligning the reflector panels to the desired accuracy is a very important task which becomes relatively simple for the flat reflectors. The parabolic reflector can for instance be measured and aligned by triangulation using two telescopes mounted in positions A and B on the antenna. A small computer coupled to the telescopes quickly determines the deviation from the theoretical surface. A and B are supports whose location can be easily and accurately determined, and from which the parabolic reflector can always be seen equally well when rotated in elevation. Measurements of the parabolic surface can therefore be made for any elevation angle of the antenna, a very valuable feature unique to this antenna design.

III. ELECTRICAL SCALE MODEL TESTS

3.1 *The Antenna Model*

Analytic investigation of the triply-folded conical horn-reflector antenna is a formidable problem involving the solution of the propagation equations in the oversized conical waveguide represented by the folded horn. Electrical scale model testing, however, has been shown to be valuable in assessing the electrical characteristics of large antennas.[2] In the present case, the availability of a precision conical horn-reflector antenna model minimized the fabrication cost but dictated the size of the model.

In order to make direct comparison between folded and straight conical horn-reflector antennas, the model was constructed so that the precision parabolic reflector section could be attached to either the folded or the straight conical horn. Fig. 4 is a scaled cross section drawing of the folded conical horn-reflector model with pertinent dimensions. Shown by dotted lines is the position of the straight conical horn when attached to the reflector. The model has a focal length of 24 inches and a flare angle of 31.5 degrees. The RMS error of the parabolic surface of this model is about 0.002 inch which, according to Ruze[4] will not cause more than 0.05 decibels reduction in gain from the theoretical value at the highest measuring frequency of 60 gc.

The original conical horn-reflector model was fabricated of thin sheet brass while the folded conical horn was machined from aluminum castings. Flat precision aluminum plates were attached as fold reflectors. Each fold section may be replaced by a straight conical section thus permitting investigation of a single fold or combination of folds. Conical horn feeds for both the TE_{11} and TM_{01} modes were provided separately.

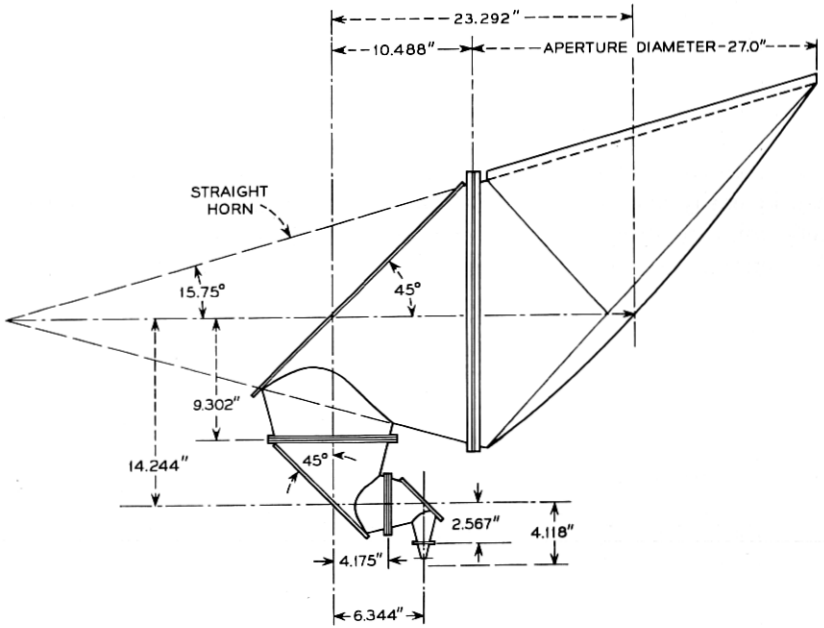

Fig. 4 — Conical horn-reflector antenna model employed for electrical tests showing pertinent dimensions of the inner surface.

Fig. 5 is a photograph of the triply-folded conical horn-reflector antenna model mounted for pattern measurements.

Aside from having a greater flare angle (31.5 vs 25 degrees) than the antenna in Fig. 2, the aperture diameter of the model is undersized by a factor of 1.6. This factor is based on the assumption that the ground station antenna of Fig. 2 would operate at 4 gc vs a 60 gc measuring frequency for the model. Both the larger flare angle and the undersized scale enhance the diffraction effects of the folds in the model compared with the antenna of Fig. 2. The model measurements should therefore give a somewhat pessimistic answer to the diffraction problems in the triply-folded horn.

4.2 *The Measuring Technique*

One purpose of the electrical measurements was to obtain far field radiation patterns having sufficient accuracy to be employed in the analytical determination of gain and noise temperature of the model. Sufficient accuracy is obtained by measuring at least 30 decibels below

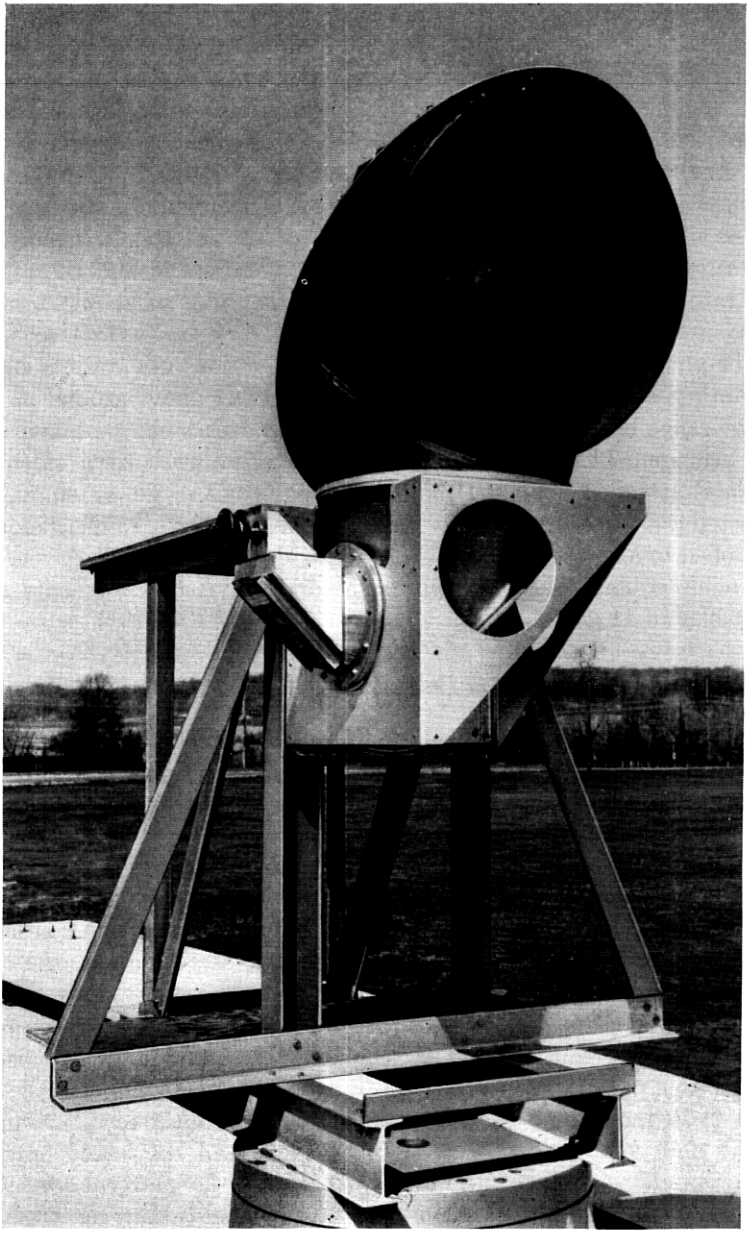

Fig. 5 — The antenna model mounted for radiation pattern measurements in the transverse plane and 0° elevation.

the isotropic level of the antenna. Since the gain of this antenna at 60 gc is about 51 decibels, an 81-decibel dynamic measuring range is required. This range is achieved through the use of a high-power short pulse technique. The short pulse technique allows both the elimination of spurious reflections from outside the direct signal path and a wide dynamic range. Otherwise, standard antenna measuring procedures are employed at the 1500-foot antenna range of the Holmdel Laboratory.

The signal source consists of a 10-kw peak power output magnetron operating at 60 gc. The pulse width is 0.2 microsecond and the repetition rate 1000 cps. A 30-decibel rectangular horn located about 12 inches above ground is used as a source antenna.

The antenna model can be mounted with various orientations on an azimuth positioner which is located about 30 feet above ground on top of the range building. Complete 360 degree patterns can be taken with this arrangement. A superheterodyne receiver followed by a video detector is attached to the output waveguide of the model antenna. The detected pulse is amplified in a narrow band 1000-cps amplifier before it is applied to a rectangular, logarithmic pattern recorder.

Similar equipment is also provided for pattern measurements at a frequency of 11 gc.

3.3 *The Measured Radiation Patterns*

All the pattern measurements for the TE_{11} mode were taken in the two principal planes (longitudinal and transverse) with linear field polarization in the same two planes. Cross polarized patterns were not taken. The planes are defined with respect to the straight horn-reflector antenna. The longitudinal plane contains the axis of the cone and the beam while the transverse plane contains the axis of the beam but is normal to the axis of the cone. The folded-horn antenna requires an additional designation to describe the rotation of the parabolic section about the cone axis. In practice this is the elevation angle of the beam with respect to the horizontal plane of Fig. 2. In the zenith or 90 degree elevation position, both the beam axis and the segments of the folded cone axis are in the same plane.

Over 30 radiation patterns were taken. These include all principal planes and polarizations of both the straight and the folded horn-reflector antennas at 60 gc and 11 gc. Only a few of the patterns are shown here. Fig. 6(a) shows a pattern for the straight horn-reflector antenna in the longitudinal plane with longitudinal polarization. The characteristic spillover lobe is clearly visible at about 70 degrees to the

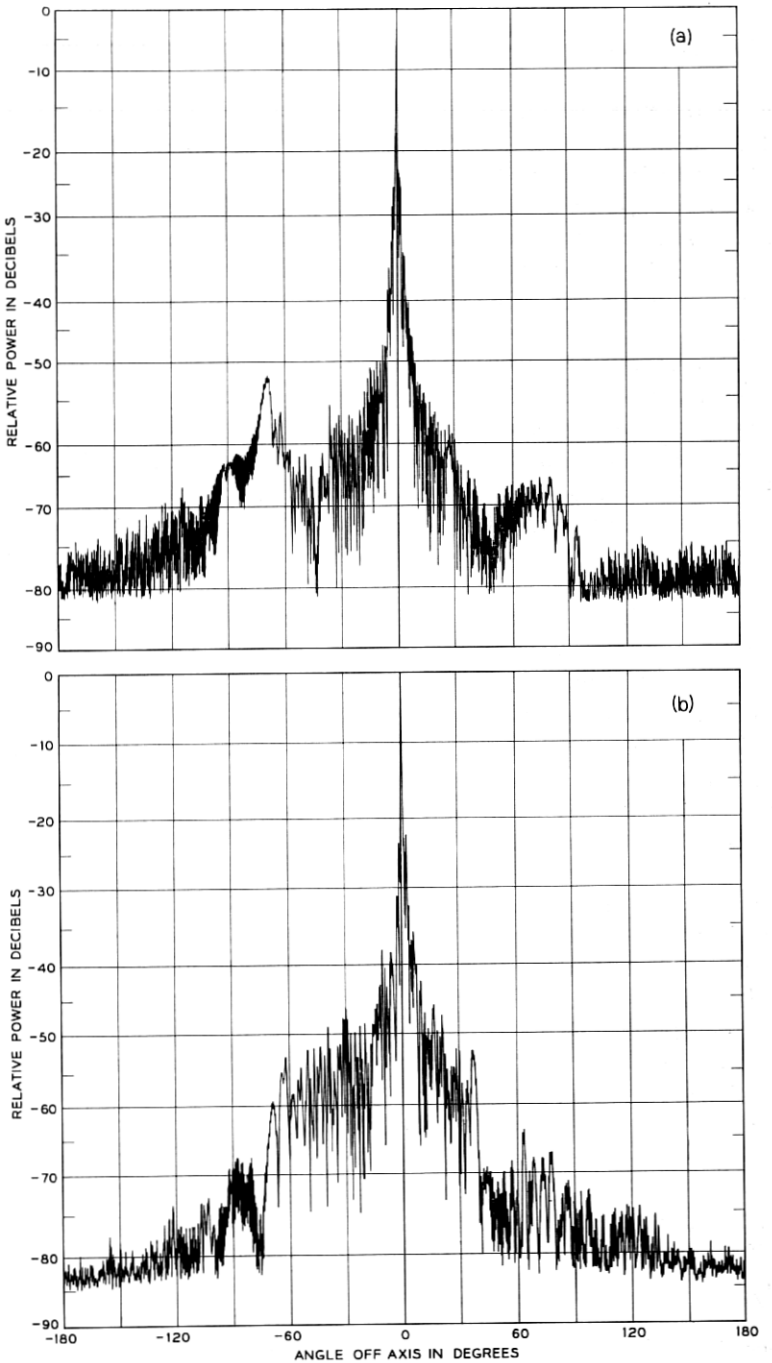

Fig. 6 — Measured radiation patterns for the TE_{11} mode in the longitudinal plane with longitudinal polarization at 60 gc: (a) straight horn (note the characteristic spillover lobe to the left of the main beam); (b) triply-folded horn in the zenith position.

left of the main beam, approaching the isotropic level of the antenna, 51 decibels. The same pattern was taken with the triply-folded horn antenna in the zenith position and is shown by Fig. 6(b). The spillover lobe has disappeared but other sidelobes closer to the main beam have become stronger. In Figs. 7(a) to 7(d), the patterns show a development of the radiation characteristics of the triply-folded horn from the straight horn. The single fold is the large area fold nearest the parabolic section. A strong spillover lobe which first becomes visible after the addition of the second fold appears at 62 degrees left of center and eventually reaches a level 6 decibels above isotropic. Of the many patterns taken, Fig. 7(d) shows the most pronounced effect of fold diffraction. In the horizon or 0 degree elevation position (not shown), the spillover lobe has practically disappeared. Fig. 8 shows an expanded section around the main beam of the pattern in Fig. 7(d). This expanded pattern has a first lobe level on the right side which is about 22 decibels below the peak. The one on the left side, however, has actually moved into the main beam. The computed pattern for the straight horn-reflector antenna gives the first sidelobe level as -24 decibels and a null depth of -26 decibels between the main beam and first sidelobe.[2]

For any satellite station application, the triply-folded horn must be equipped with an automatic tracking system similar to the one used at the Andover satellite station.[5] Since such a tracking system makes use of the TM_{01} mode, the TM_{01} radiation patterns of the triply-folded horn-reflector antenna model were measured. The results are presented in Fig. 9 together with the corresponding TE_{11} mode patterns. The peak levels of the two patterns were made equal, although the TM_{01} maxima were actually 5 decibels below the TE_{11} maxima. It is observed that the four TM_{01} mode patterns are quite symmetrical and that their nulls which are at least 28 decibels deep, align well with the peaks of the TE_{11} mode patterns.

In order to obtain a feeling for the amount of misalignment which could be tolerated in a triply-folded horn antenna, deliberate angular errors were introduced in the three axes segments of the folded conical horn. Pattern measurements indicate that errors in the amount of one beamwidth (0.5 degrees) in each segment do not cause serious degradation of the antenna characteristics. Aside from some expected beam-shifting, the main beam width of the TE_{11} mode patterns increases slightly while the TM_{01} mode patterns suffer from decreased null depth.

Pattern measurements at 11 gc, which are not included here, show increased diffraction effects due to the folds especially in the vicinity of the main beam. A general survey of all the available principal radiation

patterns indicates that a certain degradation of the antenna characteristics has taken place by introducing the three folds in the horn. This degradation can only be realistically judged by comparing the gain and noise temperature of the two types of antennas.

3.4 *Gain and Noise Temperature*

The accuracy of the standard horn comparison technique for gain determination was found to be inferior to the pattern integration method.

Both gain and antenna noise temperature were therefore computed by means of the following expressions which are derived in Appendix A:

$$G_0 = \frac{4\pi}{\int_{\theta=0}^{\pi}\int_{\phi=0}^{2\pi} P_n(\theta,\phi)\ \sin\theta d\theta d\phi} \tag{1}$$

and

$$T_A = \frac{G_0}{4\pi}\int_{\theta=0}^{\pi}\int_{\phi=0}^{2\pi} P_n(\theta,\phi)\,T(\theta,\phi)\ \sin\theta d\theta d\phi \tag{2}$$

where ϕ and θ are spherical coordinates with $\theta = 0$ coincident with the electrical axis of the antenna. Pattern measurements yield directly the normalized gain function $P_n(\theta,\phi) = P(\theta,\phi)/P(0,0)$. For temperature calculations, the temperature, $T(\theta,\phi)$, of the sphere surrounding the antenna has to be specified.

As explained in Appendix A, P_n consists of the sum of the principal and cross polarized radiation patterns. In the following computations, however, the cross polarized patterns were omitted, having not been measured. It is estimated that the inclusion of the cross polarized component would reduce the gain by about 0.1 decibel.

Equation (1) holds separately for the transverse and longitudinal linear polarizations used in the tests. For each polarization, the two patterns in the transverse and in the longitudinal planes are available for a total of four half patterns. Each half pattern is then assumed to encompass the 90 degree sector about the main beam axis and centered on the measured half pattern. This assumption permits the integration in ϕ to be carried out easily. The integration in θ is then performed using standard graphical techniques. Finally, the integrated patterns for transverse and longitudinal polarizations are averaged. Results of such computations are shown in Table I.

The theoretical gain values shown in Table I are calculated by the formula:

$$G = \eta(4\pi A/\lambda^2) \tag{3}$$

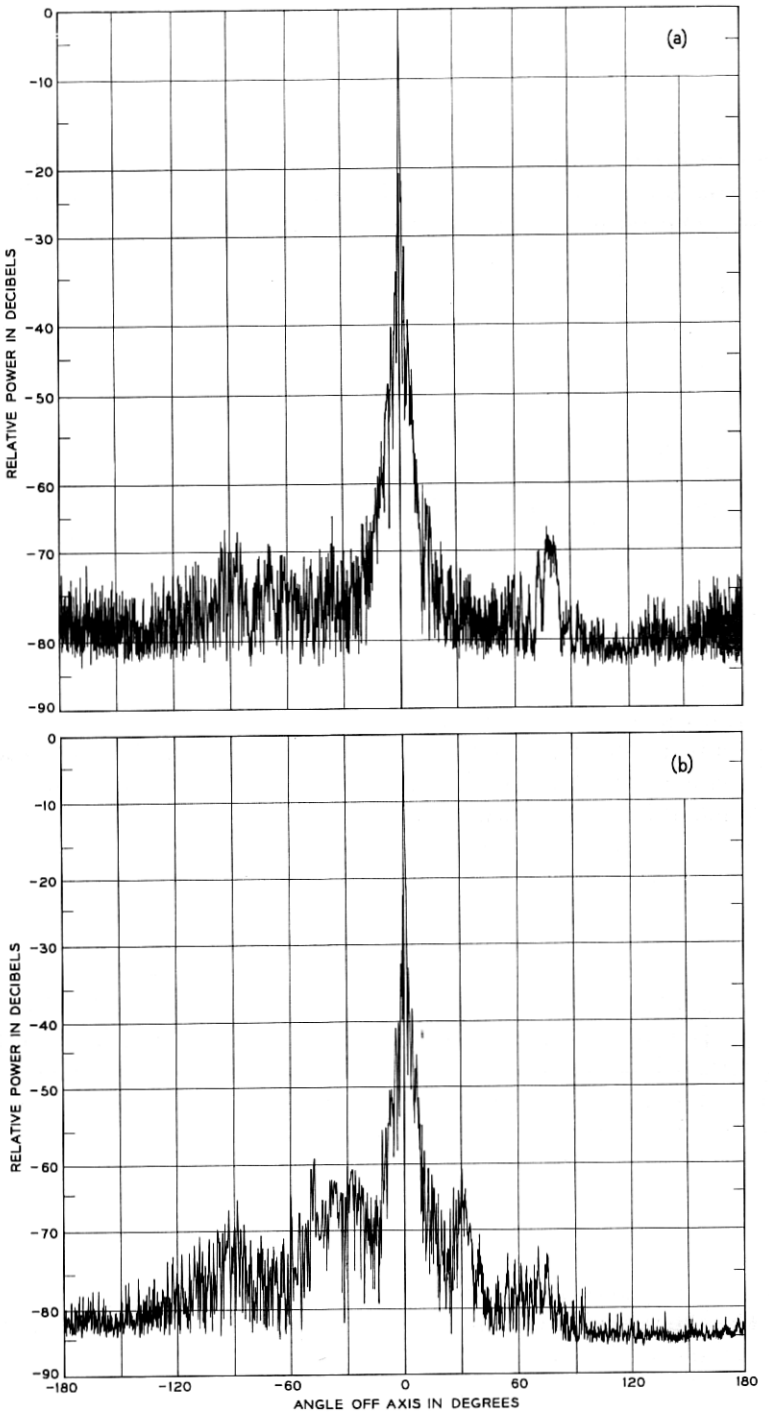

Fig. 7 — Measured radiation patterns for the TE_{11} mode in the longitudinal plane with transverse polarization at 60 gc showing the effect of progressive folding: (a) straight horn; (b) single large area fold; (c) double fold; (d) triple fold. The zenith position was used in all folded cases.

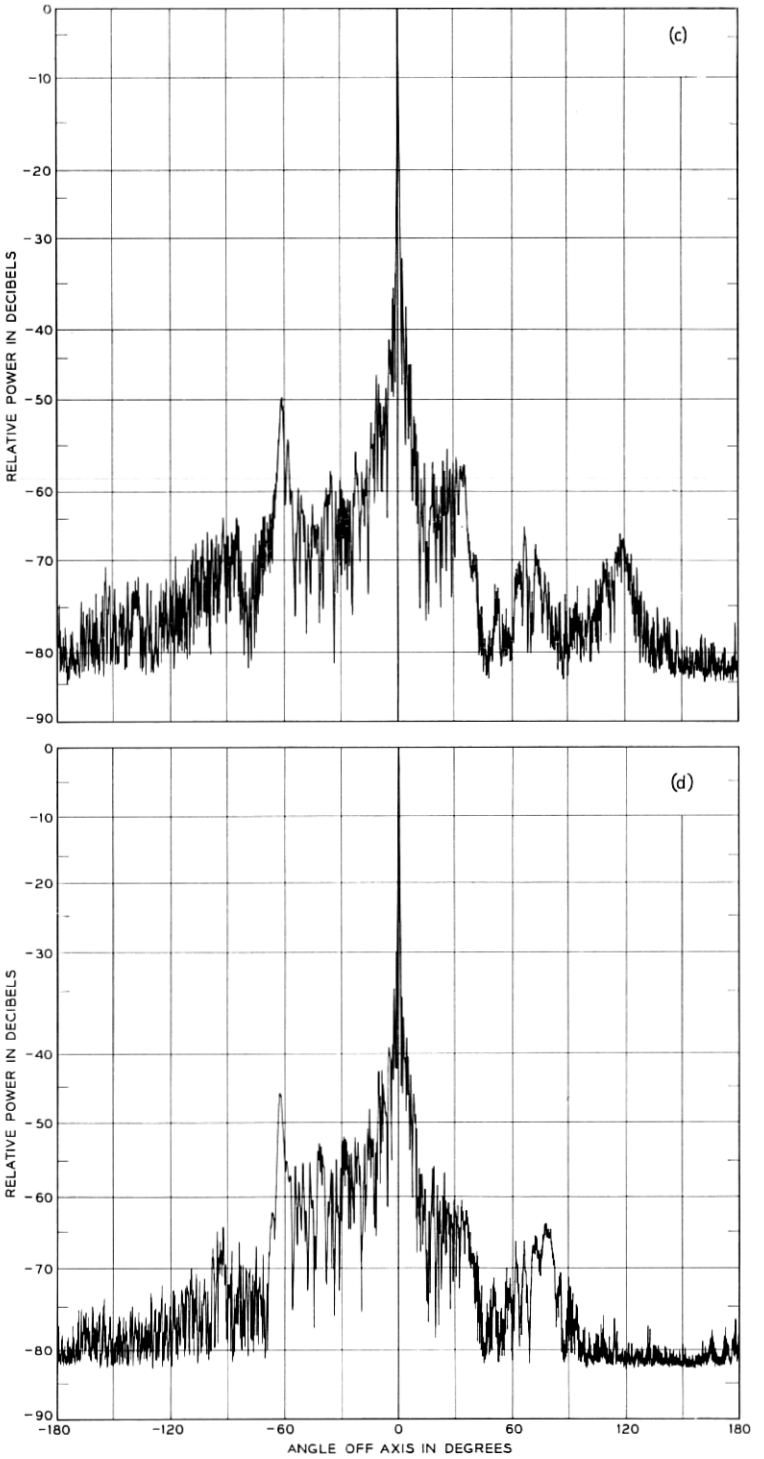
(c)
(d)
RELATIVE POWER IN DECIBELS
0
-10
-20
-30
-40
-50
-60
-70
-80
-90
-180
-120
-60
0
60
120
180
ANGLE OFF AXIS IN DEGREES

FIG. 7 (cont.)

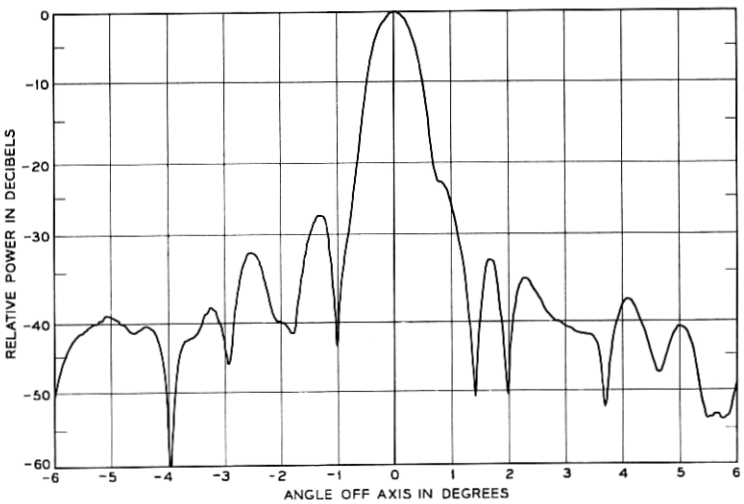

Fig. 8 — Expanded radiation pattern of Fig. 7(d) centered on the main beam and showing the first few side lobes.

where the efficiency η of the antenna aperture A is calculated to be 80.65 per cent for the conical horn-reflector antenna[2] if the effect of the characteristic spillover lobe is not taken into account. Spillover reduces the gain by approximately 0.2 decibel resulting in an efficiency of 77.1 per cent. Equation (3) and the gain values in Table I allow the calculation of antenna aperture efficiencies. For the triply-folded horn an efficiency of 60 $\pm$ 4 per cent at 60 gc is obtained practically independent of the elevation angle of the parabolic reflector. This is one decibel below the measured straight horn efficiency of 75.4 $\pm$ 5 per cent. It is expected that in an exact scaled model of the antenna of Fig. 2 the aperture efficiency would be higher and would come closer to the value of the straight horn antenna.

The antenna temperature, T_A, of (2) is computed for both the zenith position and an angle of 5 degrees above the horizon. For the zenith computation the temperature of the surrounding sphere can be assumed circularly symmetric about a normal to the earth surface. The assumed temperature distribution with elevation is:

$$T = \frac{2.2°K}{\cos \theta} \qquad 0 < \theta < 87.5° \tag{4}$$

and

$$T = 300°K \qquad 87.5° < \theta < 180°. \tag{5}$$

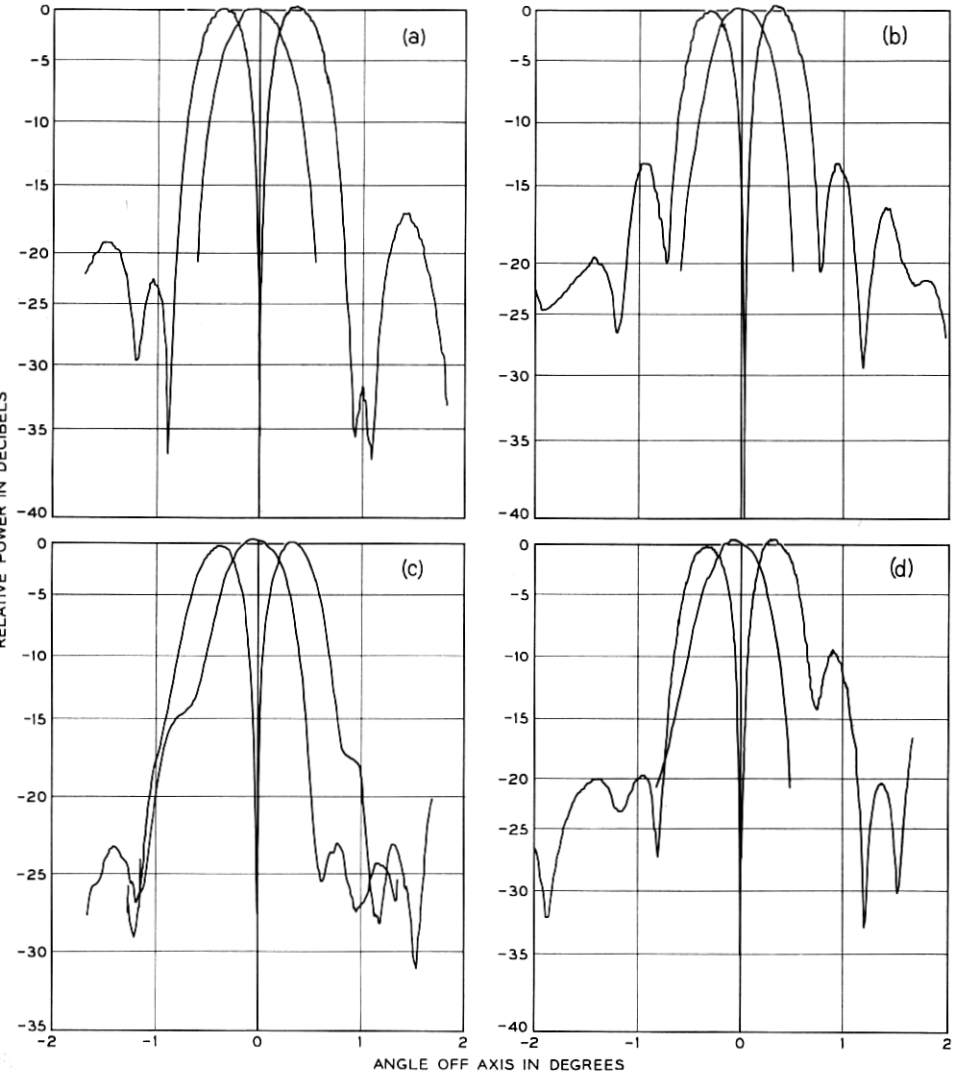

Fig. 9 — Measured radiation patterns of the triply-folded conical horn-reflector antenna model for the TM_{01} mode shown for comparison with the TE_{11} mode measured patterns. The pattern maximas have been normalized for display convenience. The measurement plane and polarization designations are: (a) transverse plane, transverse polarization and 0° position; (b) transverse plane, transverse polarization and 90° position; (c) longitudinal plane, longitudinal polarization and 0° position; and, (d) longitudinal plane, longitudinal polarization and 90° position.

TABLE I

GAINS OF THE ANTENNA MODEL DETERMINED BY INTEGRATION OF MEASURED PATTERNS

Antenna Elevation Degrees	f gc	Theoretical		Straight Horn		Triply-Folded Horn		Gain Difference Between Straight Horn and Triply-Folded Horn
		Gain db	Efficiency %	Gain db	Efficiency %	Gain db	Efficiency %	db
90	60.0	51.55	77.1	51.45	75.4	50.46	60.0	0.99
0	60.0	51.55	77.1	51.45	75.4	50.42	59.4	1.03
90	11.07	36.86	77.1	36.50	71.0	35.55	57.0	0.95
0	11.07	36.86	77.1	36.50	71.0	35.35	54.4	1.15
ONE SIGMA ERROR				±0.3	±5.0	±0.3	±4.0	±0.1

Equation (4) is a good expression for the atmospheric noise at a frequency of about 4 gc from zenith down to 2.5 degrees elevation. Below this elevation the beginning of the warm earth is assumed with a uniform temperature of 300 degrees Kelvin. This is a pessimistic assumption since the effective ground temperature will always be below 300 degrees K depending on the reflection coefficient of the earth's surface surrounding the antenna.

For an antenna elevation angle of 7.5 degrees (5 degrees above the physical horizon), the temperature distribution given by (4) and (5) was modified to simplify the integration of (2). This spherical temperature distribution can be described by two regions. The first is a spherical cap centered on the main beam described by $0 < \theta < 5°$ and consisting of atmospheric temperature only. This region is further divided into two semi-caps by a great circle arc tangential to the 7.5 degree elevation. The upper semi-cap has a temperature distribution:

$$T = \frac{2.2°K}{\cos\,(82.5° - \theta)} \quad \text{for} \quad 0 < \theta < 5° \qquad 0 < \phi < 180°. \tag{6}$$

The lower semi-cap extending below the 7.5 degree elevation line has a temperature distribution:

$$T = \frac{2.2°K}{\cos\,(82.5° + \theta)} \quad \text{for} \quad 0 < \theta < 5° \qquad 180° < \phi < 360°. \tag{7}$$

The second region may also be divided into two parts. The lower one represents the warm earth and is bounded by $5° < \theta < 180°$ and $180° < \phi < 360°$. The upper part extending toward the zenith completes the temperature sphere and is assumed to be at 0 degrees K. Results of temperature computations are shown in Table II in the form of excess antenna temperatures which are obtained by subtracting the atmospheric background temperature T_B given by (4) at the center of the main beam from T_A.

The zenith excess temperatures are very small in all cases considered, even for the triply-folded horn at 11 gc. At the lower elevation angle and 60 gc the triply-folded horn picks up about 3.9 degrees K more noise than the straight horn. At 11 gc the higher side lobe levels of the folded horn cause the noise to increase considerably at the lower elevation angle. Whereas the strong diffraction in the triply-folded horn at 11 gc did not manifest itself in a noticeable gain reduction, it shows up as a substantial increase in the noise temperature of the antenna at the lower elevation.

IV. HYDRODYNAMIC SCALE MODEL TESTS

The behavior of the antenna shown in Fig. 2 under conditions of heavy wind was determined by means of scale (1:96) model tests in water since wind-tunnel tests would have been less convenient. The measuring technique used at the hydrodynamic test facilities of the Davidson Laboratory of Stevens Institute of Technology, Hoboken, New Jersey is described elsewhere.[6] The most significant quantity measured was the azimuth wind torque coefficient C_w of the antenna. This quantity is defined by

$$T(t) = C_w V^2(t) \tag{8}$$

TABLE II

NOISE TEMPERATURES OF THE ANTENNA MODEL DETERMINED BY INTEGRATION OF MEASURED PATTERNS

Antenna Elevation Degrees	Antenna Angle Above Physical Horizon Degrees	f gc	Background Temp. °K	Straight Horn Excess Temp. °K	Triply-Folded Horn Excess Temp. °K	Excess Temp. Difference between Straight Horn and Triply-Folded Horn °K
90	87.5	60.0	2.20	0.46	0.46	0
7.5	5	60.0	16.86	4.20	8.08	3.88
90	87.5	11.07	2.20	0.45	0.79	0.34
7.5	5	11.07	16.86	13.64	89.49	75.85

where T = wind torque about the azimuth axis and V = wind velocity. C_w is a function of the wind direction and the antenna elevation. The highest value of C_w is obtained when the wind blows directly into the antenna aperture at 0 degrees elevation. This value is listed in Table III, for the triply-folded horn with and without aperture cover and for a 2250 ft.^{2} Andover-type horn-reflector antenna for comparison.

Wind induced torque about the elevation axis is small and presents no problem in tracking. The antenna overturning stability is described in terms of an overturning moment coefficient C_{wo} defined for an axis located in the base of the structure. The maximum value of C_{wo} for the most unfavorable orientation of the antenna is also given in Table III. Approximately 18×10^6 ft.-lbs. of torque is required to overturn the antenna. This estimate is based upon an estimated weight of 475,000 lbs and gives a safety factor of approximately 6 for 100 mph winds.

Calculations made by K. N. Coyne[6] give the wind speed at which the antenna stops tracking (worst case). This wind speed at stall is shown in Table III. The data is based on dual 25-hp hydraulic azimuth drives, which result in a maximum azimuth drive torque of 1.2×10^6 ft.-lbs. The table finally gives the wind velocity at which an RMS tracking error of 0.01° is reached. The assumption is made that a servo-system in the autotrack mode similar to the one used in the Andover satellite station is used.[7] The numbers indicate that negligible tracking errors are produced by winds up to 60 mph for the triply-folded horn and that the antenna can be stalled only by winds of about 80 mph or more. Comparing these numbers with those for an Andover-type antenna, one finds a very substantial improvement.

TABLE III

WIND LOAD CHARACTERISTICS OF ANTENNAS WITH 2250 FT.^{2} APERTURE

	Triply-Folded Horn		Andover Type Horn Reflector Without Radome**
	With Aperture Cover	Without Aperture Cover	
Maximum C_w in ft.-lbs./mph^2	132	184	500
Maximum C_{wo} in ft.-lbs./mph^2	156	309	—
Avg. Wind speed* for stall (at max. C_w) in mph	95	80	49
Avg. Wind speed* for 0.01° RMS autotrack error (at max. C_w) in mph	66	56	36.5

* Standard deviation of variable wind component assumed to be 30% of average velocity.

** Numbers based on wind tunnel tests.

V. SUMMARY AND CONCLUSIONS

The triply-folded conical horn-reflector antenna has been shown to be a compact antenna suitable for use in large ground stations for satellite communications. Measurements on an electrical model of the antenna indicate that the aperture efficiency of a full sized antenna should be higher than 60 per cent, which exceeds that of many existing low noise parabolic or cassegrain antennas and approaches that of the straight horn-reflector antenna. The zenith excess noise temperature of the folded horn due to side and back lobes is below 1 degree K, and, at an elevation angle of 7.5 degrees, the temperature does not exceed the very low value of the straight horn-reflector antenna by more than a few degrees. The noise temperature of a ground station containing a triply-folded horn will therefore be determined almost exclusively by circuit and atmospheric noise.

No degradation in the characteristics of the antenna is expected if the reflecting plates are aligned in angle to better than the half power width of the antenna beam. The required overall surface tolerance has to be distributed among the four reflecting surfaces. It is expected that the three flat reflectors can be easily built with high accuracy so that most of the available tolerance can be assigned to the parabolic reflector. The surface accuracy of the latter can be checked easily at any desired elevation angle by an optical triangulation method.

The compactness of the antenna and the rounded silhouette achieved by attaching lightweight fairings allows operation without a radome. Hydrodynamic model tests show that an antenna with a 2250 ft.^{2} aperture should be capable of tracking accurately up to wind velocities of more than 60 mph.

It can be said that the triply-folded horn-reflector antenna has achieved the desirable features of low-noise, high-gain, broadband operation and interference immunity because the signal path from the stationary equipment room to the parabolic reflector is entirely enclosed by a metallic sheath of considerable diameter and that this path is not folded back on itself. Some of the mentioned electrical characteristics can only be obtained in other antenna configurations by careful subreflector or beam (higher order modes) shaping. Broadband operation of such antennas is not achieved easily if at all. Construction of the triply-folded horn should also be simplified because it has only one curved reflector surface compared with at least two for cassegrain types.

VI. ACKNOWLEDGMENTS

We would like to extend our appreciation to Messrs. R. D. Peterson and T. B. Henry for measuring the radiation patterns and performing

the numerical integrations. Also to A. O. Schwarz and K. L. Warthman who modified the existing antenna model and built the folded sections. A. O. Schwarz's contributions in the mechanical area and K. N. Coyne's results of the hydrodynamic model testing have been used in writing this paper. The constant interest and support given by Messrs. I. Welber and H. P. Kelly is gratefully acknowledged.

APPENDIX A

Derivation of the Gain and Temperature Formulas

A.1 *The Antenna Gain*

According to Silver[8] the gain function of an antenna is defined by

$$G(\theta,\phi) = \frac{P(\theta,\phi)}{\frac{1}{4\pi} P_t} \tag{9}$$

where $P(\theta,\phi)$ = the power radiated per unit solid angle in direction θ,ϕ.
P_t = total power delivered to the (lossless) antenna in a single mode.

P_t obviously is the average of $P(\theta,\phi)$ integrated over the whole sphere.

$$P_t = \int_{\theta=0}^{\pi} \int_{\phi=0}^{2\pi} P(\theta,\phi) \sin\theta \, d\theta d\phi. \tag{10}$$

The denominator of (9), $P_t/4\pi$, can be interpreted as being the power radiated per unit solid angle from an isotropic antenna which is fed the total power P_t. It is convenient to write $P(\theta,\phi)$ as the sum of two orthogonal (meaning completely decoupled) components:

$$P(\theta,\phi) = P_p(\theta,\phi) + P_c(\theta,\phi), \tag{11}$$

P_p being the principal and P_c the cross-polarized component. P_p and P_c could for instance, be horizontally and vertically or right- and left-hand circularly polarized components to mention only a few out of an infinite number of possibilities.

The definition given by (9) obviously assumes that all the power $P(\theta,\phi)$ can be usefully extracted by a distant receiving antenna. This means that it is capable of receiving both components P_p and P_c, or that its polarization is matched exactly to the incoming wave. In many practical applications this requirement is easily met, e.g., a horn-reflector antenna fed by a single TE_{11} mode radiates pure linear polariza-

tion on the beam axis (but not in all other directions) and a properly aligned linearly polarized receiving antenna can extract all the possible energy. If such a match is not provided, a polarization loss occurs by which the gain given by (9) will have to be reduced.

Of particular interest is the maximum value of the gain function. We assume it occurs at $\theta = 0, \phi = 0$ and is normally called the "gain" G_0 of the antenna. Inserting (10) in (9) we obtain

$$G_0 = \frac{4\pi P(0,0)}{\int\int P(\theta,\phi) \sin \theta d\theta d\phi}. \tag{12}$$

If we introduce the "normalized" radiation function

$$P_n(\theta,\phi) = \frac{P(\theta,\phi)}{P(0,0)} \tag{13}$$

we can write (12):

$$G_0 = \frac{4\pi}{\int_{\theta=0}^{\pi}\int_{\phi=0}^{2\pi} P_n(\theta,\phi) \sin \theta d\theta d\phi}. \tag{14}$$

In general, $P_n(\theta,\phi)$ cannot be directly measured. It is much easier to determine the orthogonal components P_{np} and P_{nc} since they are the direct result of pattern measurements. We have

$$P_n(\theta,\phi) = P_{np}(\theta,\phi) + P_{nc}(\theta,\phi) \tag{15}$$

where

$$P_{np}(\theta,\phi) = \frac{P_p(\theta,\phi)}{P_p(0,0) + P_c(0,0)}$$

$$P_{nc}(\theta,\phi) = \frac{P_c(\theta,\phi)}{P_p(0,0) + P_c(0,0)}.$$

And finally, it would be easy to derive the following useful form for (9):

$$G(\theta,\phi) = G_0 P_n(\theta,\phi). \tag{16}$$

A.2 *The Antenna Temperature*

We assume that the antenna is fed in such a way as to produce the orthogonal far field intensities $P_p(\theta,\phi)$ and $P_c(\theta,\phi)$. The noise power radiated by the surrounding sphere in the matching orthogonal polarizations is proportional to the temperatures $T_p(\theta,\phi)$ and $T_c(\theta,\phi)$ existing

on the sphere. The noise power picked up by the antenna as a receiver is $W = kT_AB$, where

$$\begin{aligned} k &= \text{Boltzmann's constant} \\ B &= \text{noise bandwidth} \\ T_A &= \text{effective antenna temperature} \\ &= c\int_{\theta=0}^{\pi}\int_{\phi=0}^{2\pi} T_p(\theta,\phi)P_p(\theta,\phi)\sin\theta d\theta d\phi \\ &\quad + c\int_{\theta=0}^{\pi}\int_{\phi=\theta}^{2\pi} T_c(\theta,\phi)P_c(\theta,\phi)\sin\theta d\theta d\phi. \end{aligned} \tag{17}$$

Equation (17) immediately follows from the fact that the noise received by the antenna must be weighted by $P(\theta,\phi)$. The constant c can be easily determined if we assume the special case of a black-body enclosure, randomly polarized, at the constant temperature T_0, i.e.,

$$T_p = T_c = T_0$$

then we obtain from (17):

$$T_A = cT_0\int\int [P_p(\theta,\phi) + P_c(\theta,\phi)]\sin\theta d\theta d\phi. \tag{18}$$

Let us assume now that the antenna is perfectly matched into a termination and that it is perfectly insulated from any thermal heat sources. Then under thermal equilibrium the termination will accept the temperature of the black-body enclosure, T_0, and the noise powers coming from and flowing towards the antenna are both the same and equal to $W = kT_0B$. In practice it is impossible to find such an equilibrium between the antenna termination and the radiating enclosure. The termination can be warmer or colder depending on the input temperature of the receiver connected to the antenna. The noise powers flowing to and from the antenna are different in this case. We are only interested in the flow of noise energy coming from the antenna which for all practical purposes is still kT_0B. This means $T_A = T_0$ in (18) and we immediately find:

$$c^{-1} = \int\int [P_p(\theta,\phi) + P_c(\theta,\phi)]\sin\theta d\theta d\phi. \tag{19}$$

From (11) and (12), we find that expression (18) is also identical to

$$c^{-1} = \frac{4\pi P(0,0)}{G_0}.$$

Equation (17) now becomes:

$$T_A = \frac{G_0}{4\pi} \int_{\theta=0}^{\pi} \int_{\phi=0}^{2\pi} [T_p(\theta,\phi) P_{np}(\theta,\phi) + T_c(\theta,\phi) P_{nc}(\theta,\phi)] \sin\theta d\theta d\phi. \quad (20)$$

This expression is useful in radio astronomy where radio sources are not always randomly polarized.

For the determination of the antenna noise in a satellite communications system, it is sufficient to assume randomly polarized surroundings. This is a simplification of the physical reality which will lead to a high (pessimistic) estimate of T_A. For random noise polarization, $T_p = T_c = T$, we obtain for (20) by using (15):

$$T_A = \frac{G_0}{4\pi} \int_{\theta=0}^{\pi} \int_{\phi=0}^{2\pi} T(\theta,\phi) P_n(\theta,\phi) \sin\theta d\theta d\phi. \quad (21)$$

And with (16) we obtain the often used form:

$$T_A = \frac{1}{4\pi} \int_{\theta=0}^{\pi} \int_{\phi=0}^{2\pi} T(\theta,\phi) G(\theta,\phi) \sin\theta d\theta d\phi. \quad (22)$$

REFERENCES

1. Crawford, A. B., Hogg, D. C., and Hunt, L. E., A Horn-Reflector Antenna for Space Communication, B.S.T.J., *40*, July 1961, pp. 1095–1116.
2. Hines, J. N., Li, Tingye, and Turrin, R. H., The Electrical Characteristics of the Conical Horn-Reflector Antenna, B.S.T.J., *42*, July, 1963, pp. 1185–1211.
3. Dolling, J. C., Blackmore, R. W., Kindermann, W. J., and Woodard, K. B., The Mechanical Design of the Conical Horn-Reflector Antenna and Radome, B.S.T.J., *42*, July 1963, pp. 1137–1186.
4. Annals of the New York Academy of Sciences, *Large Steerable Radio Antennas — Climatological and Aerodynamic Considerations, 116,* June 26, 1964, discussion by J. Ruze.
5. Cook, J. S., and Lowell, R., The Autotrack System, B.S.T.J., *42*, July 1963, pp. 1283–1307.
6. Coyne, K. N., Hydrodynamic Techniques for Study of Wind Effects on Antenna Structures, B.S.T.J. this issue, pp. 1339–1365.
7. Lozier, J. C., Norton, J. A., and Iwama, M., The Servo System for Antenna Positioning, B.S.T.J., *42*, July 1963, pp. 1253–1281.
8. Silver, S., *Microwave Antenna Theory and Design,* Rad. Lab Series, *12*.